

Engineering Applications of Computational Fluid Mechanics

ISSN: (Print) (Online) Journal homepage: www.tandfonline.com/journals/tcfm20

Energy and cost management of different mixing ratios and morphologies on mono and hybrid nanofluids in collector technologies

Hai Tao, Mohammed Suleman Aldlemy, Omer A. Alawi, Haslinda Mohamed Kamar, Raad Z. Homod, Hussein A. Mohammed, Mustafa K. A. Mohammed, Abdul Rahman Mallah, Nadhir Al-Ansari & Zaher Mundher Yaseen

To cite this article: Hai Tao, Mohammed Suleman Aldlemy, Omer A. Alawi, Haslinda Mohamed Kamar, Raad Z. Homod, Hussein A. Mohammed, Mustafa K. A. Mohammed, Abdul Rahman Mallah, Nadhir Al-Ansari & Zaher Mundher Yaseen (2023) Energy and cost management of different mixing ratios and morphologies on mono and hybrid nanofluids in collector technologies, *Engineering Applications of Computational Fluid Mechanics*, 17:1, 2164620, DOI: [10.1080/19942060.2022.2164620](https://doi.org/10.1080/19942060.2022.2164620)

To link to this article: <https://doi.org/10.1080/19942060.2022.2164620>



© 2023 The Author(s). Published by Informa UK Limited, trading as Taylor & Francis Group



Published online: 24 Jan 2023.



[Submit your article to this journal](#)



Article views: 1734



[View related articles](#)



[View Crossmark data](#)



Citing articles: 4 [View citing articles](#)

Energy and cost management of different mixing ratios and morphologies on mono and hybrid nanofluids in collector technologies

Hai Tao^{a,b,c}, Mohammed Suleman Aldlemy^d, Omer A. Alawi^e, Haslinda Mohamed Kamar^e, Raad Z. Homod^f, Hussein A. Mohammed^{e,g}, Mustafa K. A. Mohammed^h, Abdul Rahman Mallahⁱ, Nadhir Al-Ansari^j and Zaher Mundher Yaseen^{k,l}

^aSchool of Computer and Information, Qiannan Normal University for Nationalities, Duyun, Guizhou, People's Republic of China; ^bCollege of Information and Artificial Intelligence, Nanchang Institute of Science and Technology, Nanchang, People's Republic of China; ^cInstitute for Big Data Analytics and Artificial Intelligence (IBDAAI), Universiti Teknologi MARA, Shah Alam, Selangor, Malaysia; ^dDepartment of Mechanical Engineering, College of Mechanical Engineering Technology, Benghazi, Libya; ^eDepartment of Thermofluids, School of Mechanical Engineering, Universiti Teknologi Malaysia, UTM Skudai, Johor Bahru, Malaysia; ^fDepartment of Oil and Gas Engineering, Basrah University for Oil and Gas, Basrah, Iraq; ^gWA School of Mines-Minerals, Energy & Chemical Engineering, Curtin University, Bentley, WA, Australia; ^hRadiological Techniques Department, Al-Mustaqbal University College, Babylon, Iraq; ⁱDepartment of Engineering, Reykjavik University, Reykjavik, Iceland; ^jCivil, Environmental and Natural Resources Engineering, Lulea University of Technology, Lulea, Sweden; ^kCivil and Environmental Engineering Department, King Fahd University of Petroleum & Minerals, Dhahran, Saudi Arabia; ^lInterdisciplinary Research Center for Membranes and Water Security, King Fahd University of Petroleum & Minerals, Dhahran, Saudi Arabia

ABSTRACT

The flat-plate solar collector (FPSC) three-dimensional (3D) model was used to numerically evaluate the energy and economic estimates. A laminar flow with $500 \leq Re \leq 1900$, an inlet temperature of 293 K, and a solar flux of 1000 W/m^2 were assumed the operating conditions. Two mono nanofluids, CuO-DW and Cu-DW, were tested with different shapes (Spherical, Cylindrical, Platelets, and Blades) and different volume fractions. Additionally, hybrid nanocomposites from CuO@Cu/DW with different shapes (Spherical, Cylindrical, Platelets and Blades), different mixing ratios (60% + 40%, 50% + 50% and 40% + 60%) and different volume fractions (1 volume%, 2 volume%, 3 volume% and 4 volume%) were compared with mono nanofluids. At 1 volume% and $Re = 1900$, CuO-Platelets demonstrated the highest pressure drop (33.312 Pa). CuO-Platelets achieved the higher thermal enhancement with (8.761%) at 1 vol.% and $Re = 1900$. CuO-Platelets reduced the size of the solar collector by 25.60%. Meanwhile, CuO@Cu-Spherical (40:60) needed a larger collector size with 16.69% at 4 vol.% and $Re = 1900$. CuO-Platelets with 967.61, CuO - Cylindrical with 976.76, Cu Platelets with 983.84, and Cu-Cylindrical with 992.92 presented the lowest total cost. Meanwhile, the total cost of CuO - Cu - Platelets with 60:40, 50:50, and 40:60 was 994.82, 996.18, and 997.70, respectively.

ARTICLE HISTORY


Received 8 November 2022
Accepted 29 December 2022


KEYWORDS

solar collector;
mono-nanofluids;
hybrid-nanofluids; thermal
performance; cost analysis

Nomenclature and acronyms

Al_2O_3	Aluminum oxide	GNPs	Graphene nanoplatelets
ASC	Solar collector area, m ²	Gr	Graphene
CeO_2	Cerium(IV) oxide	HTFs	heat transfer fluids
Co_3O_4	Cobalt oxide	IDh	inner hydraulic diameter, mm
C_p	Specific heat capacity, J/kg-K	K	Thermal conductivity, W/m-K
CTAB	Cetrimonium bromide	L	Total flat-plate length, mm
Cu	Copper	LPM	Liter Per Minute
CuO	Copper oxide	M	Nanoparticle shape factor
DW	Distilled water	\dot{m}	Mass flow rate, kg/s
Fe_3O_4	Iron(II,III) oxide	MgO	Magnesium oxide
FPSC	flat-plate solar collector	MWCNTs	Multi-Walled Carbon Nanotubes
		ODh	Outside hydraulic diameter, mm

CONTACT Zaher Mundher Yaseen  zaheryaseen88@gmail.com

 Supplemental data for this article can be accessed here. <https://doi.org/10.1080/19942060.2022.2164620>

PER	Property enhancement ratio
Pr	Prandtl number, $\left(\frac{C_p \mu}{k}\right)$
q_w''	Wall heat flux, W/m^2
Qgain/Qin	Useful energy/gain energy, W
Re	Reynolds number
SiO ₂	Silicon dioxide
t	Flat-plate thickness, mm
Tin	Inlet fluid temperature, K
TiO ₂	Titanium dioxide
Tout	Outlet fluid temperature, K
Tw-80	Tween-80
Uin	Inlet fluid velocity, m/s
w	Flat-plate width, mm
WO ₃	Tungsten trioxide
u, v, w	Velocity vectors of working fluids

Greek symbols

μ	Dynamic viscosity, kg/m-s
ΔP	Pressure drop, Pa
η_{SC}	Solar collector efficiency, %
ρ	Density, kg/m ³
φ	Nanoparticles volumetric percentage, %
Ψ	Sphericity of nanoparticles

1. Introduction

1.1. Research background and motivation

Flat plate solar collectors (FPSCs) are the most basic form of all solar collectors and have a broad array of applications, mainly in residential and industrial locations. Water and air are the standard heat transfer fluids (HTFs) circulating inside the header and riser pipes of FPSCs (Farhana et al., 2021). Water and air-based solar collectors have been the subject of much experimental, theoretical, and numerical study (Gunjo et al., 2017), (Ziyadanogullari et al., 2018). Despite its ease of production, the efficiency of the flat plate solar collector remains a source of concern and requires significant improvement (Alawi et al., 2020), (Sheikholeslami et al., 2021), (Zayed et al., 2019). A group of experts investigated the impact of various working fluids in FPSCs through experiments and simulations to enhance the heat transfer mechanism in flow pipelines (Pandey & Chaurasiya, 2017). Nanofluids (nanomaterials suspended in dispersion mediums) have recently been proposed as a passive method inside the solar collector due to their thermal performance (Dehaj & Mohiabadi, 2019). Both types of nanofluids may be utilized as mono (single nanomaterials) and nanocomposites (two or more nanomaterials) have shown superior thermal improvements when compared to basic fluids (Sint et al., 2017).

1.2. Dopted literature review on mono and hybrid nanofluids

Ziyadanogullari et al. (Ziyadanogullari et al., 2018) investigated three types of metallic oxide nanofluids (Al₂O₃, CuO, and TiO₂) as HTFs in FPSC. Their findings revealed that due to the thermal conductivity values of individual nanofluids, CuO and TiO₂ achieved higher and lower thermal performance, respectively. Four metallic-based nanofluids (SiO₂-DW, TiO₂-DW, Al₂O₃-DW, CuO-DW) and two carbon-based nanofluids (Gr-DW, and MWCNTs-DW) were experimentally examined as HTFs inside FPSC application (Verma et al., 2017). MWCNTs-DW showed higher enhancement exergy efficiency (29.32%) and energy efficiency (23.47%) relative to DW. Other nanofluids' exergy efficiency was enhanced by 21.46% for (Gr-DW), 16.67% for (CuO-DW), 10.86% for (Al₂O₃-DW), 6.97% for (TiO₂-H₂O), and 5.74% for (SiO₂-DW). Meanwhile, energy efficiency was improved by 16.93% for (Gr-DW), 12.64% for (CuO-DW), 8.28% for (Al₂O₃-DW), 5.09% for (TiO₂-H₂O), and 4.08% for (SiO₂-DW) at 0.025 kg/s and 0.75 volume%. Two carbon-based nanofluids (GNPs-DW, Gr-DW) and two metal oxides based nanofluids (Al₂O₃-DW, and SiO₂-DW) were tested in a theoretical study under the conditions of different heating rates (500, 750, and 1000 W/m²), different volumetric percentages (0.25%, 0.5%, 0.7%, and 8%), different inlet-temperatures (30°C, 40°C, and 50°C) and different mass flow rates (0.0085 kg/s, 0.017 and 0.0255 kg/s) (Liu et al., 2020). They concluded that the energy performance was enhanced by 64.45% for (SiO₂-DW), 67.03% for (Al₂O₃-DW), 72.45% for (Gr-DW), and 76.56% for (GNPs-DW). Six different water-based nanofluids (Al₂O₃-DW, CuO-DW, MWCNTs-DW, Fe₃O₄-DW, WO₃-DW, and CeO₂-DW) were investigated HTFs inside FPSC (Tong et al., 2020). The solar collector efficiency was ranged from the highest reading of 87% for MWCNTs-DW and the lowest reading of 62% for DW.

Numerous experimental and theoretical studies on the mechanisms of thermal efficiency in solar collectors have been conducted due to hybrid nanofluids' significant academic and industrial interest. Three nanofluids such as Al₂O₃-DW, TiO₂-DW, and Al₂O₃@TiO₂-DW were prepared in the presence of surfactant (CTAB) to be tested numerically and experimentally as HTFs inside FPSC (Farajzadeh et al., 2018). Meanwhile, the velocity of nanofluids was in the range of 1.5, 2.0, and 2.5 LPM. The hybrid showed higher energy effectiveness over individual nanofluids by 19% for (0.1wt.%-Al₂O₃-DW), 21% for (0.1wt.%-TiO₂-DW), and 26% for (Al₂O₃@TiO₂-DW) relative to the basic working fluid (water). Exergy efficiency was increased by 2.59%

due to the application of a hybrid nanofluid. Moreover, Additionally, the production of entropy in the nanocomposite fluid (CuO@Cu-DW) was reduced by 3.31%, that of the individual nanofluids by 1.35% (Cu-DW), and 2.96% for (CuO-DW). Two nanocomposite fluids, namely (80%-MgO + 20%-MWCNTs) and (80%-CuO + 20%-MWCNTs) were evaluated under the terms of different concentrations of 0.25–2.0% and different volume flow rates of 0.5–2.0 LPM (Verma et al., 2018). In comparison to the basic fluid, the combination of CuO@MWCNTs-DW outperformed MgO@MWCNTs-DW in terms of energy effectiveness by 20.52% and 18.05%, respectively. Maximum numerical and experimental enhancements of 8.5% and 12.8% have been observed for convective heat transfer properties using Al₂O₃@TiO₂ composite nanofluid in a mini-channel heat sink with a different mixing ratio (V. Kumar & Sarkar, 2019). Moreover, in experimental work, the influence of nanoparticle ratio on hydrothermal properties of plate heat exchanger using Al₂O₃@MWCNT hybrid nanofluids was examined. They concluded that, the hydrothermal efficiency of nanofluids increased with an increase in carbon-based-ratio due to the insignificant impact on pressure drop (Bhattad et al., 2019). Additionally, all of the nanofluids' performance evaluation criteria (PEC) scores were greater than 1 (V. Kumar & Sarkar, 2020b). Besides that, for MWCNTs nanofluid, the maximum heat transfer coefficient and pressure drop increments were 44.1% and 68.1%, respectively (V. Kumar & Sarkar, 2020a).

A triple hybrid nanosuspension (MWCNTs@GNPs with h-BN) was prepared in DW using a surfactant (Tween-80) (Hussein et al., 2020). Three different volume flow rates (2, 3, and 4 LPM) were used as their input limitations. The solar collecting efficiency reached up to 85% at 4 LPM because of employing the hybrid nanofluid. The combination of hybrid nanofluid nanodiamond@cobalt oxide (ND@Co₃O₄-DW) was produced in different percentages (0.05–0.15%) and different volume flow rates (0.56–1.35 LPM). The 0.15 weight%-hybrid nanofluid was outperformed the basic fluid by about 59% and 48%, respectively. Single and composite nanofluids (Al₂O₃-DW, Al₂O₃@Fe-DW) were examined for collector efficiency with different volume percentages (Okonkwo et al., 2020). This study, enhanced the thermal performance of 0.1 volume%-single nanofluid and 0.1 volume%-hybrid nanofluid by 2.16% and 1.79% relative to pure water. On the other hand, hybrid Al₂O₃@Fe-DW provided an exergy efficiency enhancement of 6.9% against 5.7% using a single Al₂O₃-DW. Recently, an artificial intelligence model was implemented to predict the thermal properties of single and hybrid water-based Al₂O₃ and Al₂O₃@CuO (50:50) nanofluids (Marulasiddeshi

et al., 2022). The highest increase in thermal conductivity and dynamic viscosity of 1vol.-%-hybrid nanofluid was 14.6 and 6.5% higher than 1vol.-%-single nanofluid, respectively. The radiator size and cost reduction was examined using EG and different combinations of hybrid nanofluids in the presence of various nanomaterials such as (Ag, Cu, SiC, CuO, TiO₂ and Al₂O₃) (Sahoo & Sarkar, 2016). They concluded that, radiator size was reduced by 3.7% and pumping power increased 2.9% for Ag-EG hybrid nanofluids as compared to the base fluid. Cost-effective shell and tube condenser measurements using Al₂O₃@MWCNTs hybrid nanofluid was studied (Singh & Sarkar, 2018). 1vol.-%-Al₂O₃@MWCNTs nanofluid produced maximum operating cost savings by about (11.1%), meanwhile, 1vol.-%-Al₂O₃@Ag showed a minimum (9.62%).

1.3. Research objectives and motivations

Based on the previously reported literature review, very limited research was observed on comparing mono and hybrid nanofluids inside solar collector systems. Hence, research development of this perspective is highly motivated for such a kind of nanomaterials domain. The ultimate research aim was to evaluate two mono nanofluids (CuO/ H₂O and Cu/ H₂O) and three hybrid nanofluids (i.e. (60%-CuO@40%-Cu/H₂O), (50%-CuO@50%-Cu/DW) and (40%-CuO@60%-Cu/DW)) with different nanoparticle shapes (i.e. Spherical, Cylindrical, Platelets, and Blades). Thermal-physical properties were calculated through a set of equations at 293 K. Various simulations were performed under the condition of $500 \leq Re \leq 1900$ to examine the thermal and economic performances of FPSC. The importance and originality of this study is to explore the effect of single/hybrid nanofluids, volume fractions, nanoparticle morphologies, and mixing ratios for the nanocomposites. That will substantially contribute to solar collector design with optimal energy efficiency and minimal size and cost.

2. Modeling and methods

2.1. Geometrical model

Figure 1-a describes the current physical problem of a thin flat plate made of aluminum attached to a copper riser flat-tube working under the condition of conjugated laminar mixed convection. In this model, the solar radiation was represented by constant heat flux (q'') applied at the flat plate surface. The total flat-plate length (L) of 1500 mm, flat-plate width (w) of 60 mm, flat-plate thickness (t) of 2 mm, inner hydraulic diameter (IDh) of 12.5 mm, outside hydraulic diameter (ODh) of 14.8

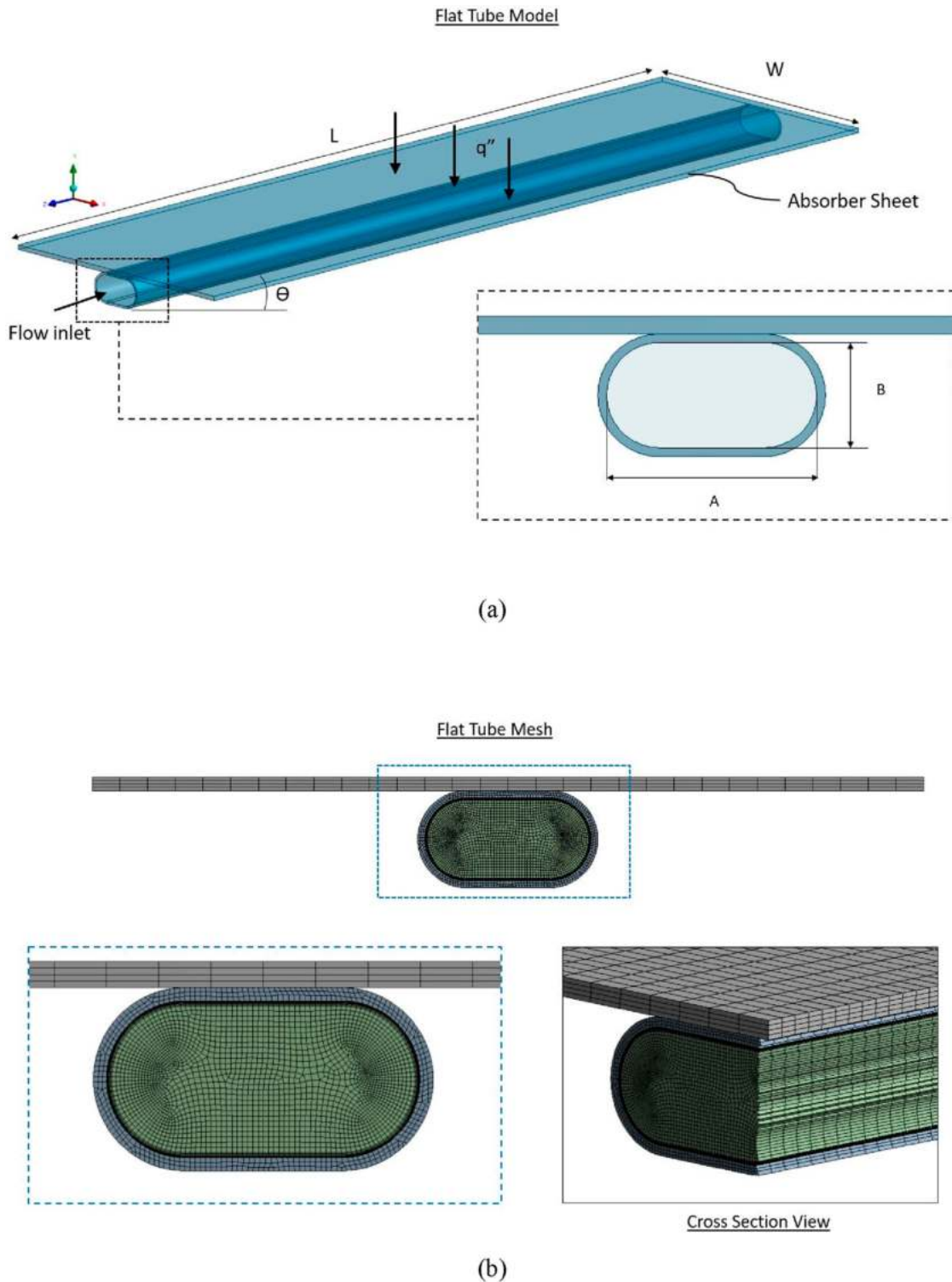


Figure 1. (a) A drawing illustration of flat plate-flat tube numerical model, (b) the computational domain and mesh topology.

mm, and wall thickness of 1 mm were adopted. The flat tube hydraulic diameter is expressed by the following formula: $(D_h = 4 \times \frac{\pi B^2 + (A-B) \times B}{\pi \times B + 2 \times (A-B)})$. The mesh structure and configurations are critical steps in adequately implementing the current physical model's analysis. The CFD domain is further subdivided into many small cells to enhance grid size management and meshing efficiency.

An unstructured grid was used for the interior volume cells. The computational grid is shown in Figure 1-b.

2.2. Numerical simulation approach

A conjugated laminar mixed convection was solved using mono (single) and hybrid (mixture) nanofluids in different types (CuO and Cu), different volumetric

percentages (1, 2, 3, and 4 volume%), different structures (Spherical, Cylindrical, Platelets and Blades) and different mixing ratios (60:40, 50:50 and 40:60). The thermo-physical properties of dispersion medium (DW), single and mixture nanomaterials were collected from the previous published work (Minea, 2017), and set of equations and mathematical models were applied to calculate the thermal properties of mono and hybrid nanofluids. The model is built on various assumptions to simplify the problem without impacting the fundamental concepts. The assumptions are given below:

- (i) The thermal system operates under the condition of steady-state.
- (ii) The base fluid and mono/hybrid nanofluid flow uniformly through all riser flat-tube of the thermal collector.
- (iii) Uniform temperature around the wall of the riser flat-tube.
- (iv) The mono and hybrid nanofluids are considered single-phase, homogeneous, and long-term stable.
- (v) A constant wall heat flux heats the thin flat-plate absorber at the value of (1000 W/m²).
- (vi) The lateral absorber plate walls and lower outer riser flat-pipe have adiabatic with non-slip boundary conditions.
- (vii) Body forces, the solar radiation model, and compressibility are ignored.

The governing equations of this problem are continuity, momentum, and energy equations, as shown in Eqs. (1-3): (Charjouei Moghadam et al., 2017), (Edalatpour & Solano, 2017):

$$\frac{\partial}{\partial x_i}(\rho u_i) = 0 \quad (1)$$

$$\frac{\partial}{\partial x_j}(u_i u_j) = \frac{\partial p}{\partial x_i} + \frac{\partial}{\partial x_j} \left(\nu \left(\frac{\partial u_i}{\partial x_j} + \frac{\partial u_j}{\partial x_i} \right) - \dot{u}_i \dot{u}_j \right) - g_i \beta (T - T_{ref}) \quad (2)$$

$$\frac{\partial \rho c_p u_j T}{\partial x_i} = \frac{\partial}{\partial x_j} \left(k \frac{\partial T}{\partial x_j} - \rho c_p u_j T \right) + S_t \quad (3)$$

In this regard, the notation of $i = 1, 2, 3$, $u_i = (u, v, w)$ refers to the velocity vectors of working fluids.

Meanwhile, the following boundary conditions are defined to complete the above mathematical equations for the computational domain (Charjouei Moghadam et al., 2017), (Edalatpour & Solano, 2017):

$$\begin{aligned} u &= v = 0, \\ w &= U_{in}, T = T_{in} \\ u &= v = w = 0 \end{aligned} \quad (4)$$

$$\begin{aligned} q''_w &= I(\lambda k) - h(T_{in} - T_{amb}) \\ u &= v = w = 0 \end{aligned} \quad (5)$$

$$\frac{\partial T}{\partial y} = 0 \quad (6)$$

$$\begin{aligned} \frac{\partial u}{\partial z} &= \frac{\partial v}{\partial z} = \frac{\partial w}{\partial z} = 0 \\ \frac{\partial T}{\partial z} &= 0 \end{aligned} \quad (7)$$

$$k \frac{\partial T}{\partial x} = k_s \frac{\partial T_s}{\partial x} \quad (8)$$

The parameters of Reynolds number (Re), Prandtl number (Pr), pressure drop (ΔP), and solar collector efficiency (η_{SC}), can be calculated as (Edalatpour & Solano, 2017), (Sarsam et al., 2020b), (Sarsam et al., 2020a):

$$Re = \left(\frac{\rho U_{in} D_h}{\mu} \right) \quad (9)$$

$$Pr = \left(\frac{C_p \mu}{k} \right) \quad (10)$$

$$\Delta P = (\bar{P}_{out} - \bar{P}_{in}) = f \frac{L}{D_h} \frac{\rho U_{in}^2}{2} \quad (11)$$

$$\eta_{SC} = \frac{Q_{Qain}}{A_{SC} q''_w} = \frac{\dot{m} C_p (T_{out} - T_{in})}{A_{SC} q''_w} \quad (12)$$

2.3. Thermophysical properties

The thermophysical properties of dispersion mediums (base fluids) such as density (ρ), dynamic viscosity (μ), specific heat capacity (C_p), and thermal conductivity (k), are greatly improved by adding nanomaterials in different nanoparticles' volumetric percentages and different nanoparticles morphologies. The thermophysical properties of DW and (CuO and Cu) nanoparticles under the conditions of 293 K and 50 nm were collected from the available literature as tabulated in Table 1 (Minea, 2017). In this study, two mono nanofluids, namely CuO-DW and Cu-DW, with different structures (Spherical-shaped, Cylindrical-shaped, Platelets-shaped, and Blades-shaped) and different volumetric percentages, were different examined. Moreover, nanocomposites from CuO@Cu-DW with other structures (Spherical,

Table 1. Thermophysical properties of dispersion medium (DW), CuO and Cu nanoparticles (50 nm) at 293 K.

DW/ Nanoparticles	Density (ρ) (kg/m ³)	Specific heat (C_p) (J/kg K)	Thermal conductivity (k) (W/m-K)	Dynamic Viscosity (μ) (kg/m-s)
DW	998.5	4182	0.602	7.9×10^{-4}
CuO	6500	533	17.65	-
Cu	8940	385	401	-

Cylindrical, Platelets, and Blades-shaped) have different mixing ratios (60%+40% 50%+50%, and 40%+60%), and different nanoparticles volumetric percentages were compared to mono nanofluids in terms of thermal performances and evaluations.

The effective density of the single (mono) and mixture (hybrid) nanofluids is written as (Benkhedda et al., 2019):

$$\rho_{nf} = (1 - \varphi)\rho_{DW} + \varphi\rho_{CuO/Cu} \quad (13-a)$$

$$\rho_{hybrid} = (1 - \varphi_{CuO} - \varphi_{Cu})\rho_{DW} + \varphi_{CuO}\rho_{CuO} + \varphi_{Cu}\rho_{Cu} \quad (13-b)$$

Also, the specific heat capacity of single (mono) and mixture (hybrid) nanofluids can be determined as (Benkhedda et al., 2019):

$$(\rho C_p)_{nf} = (1 - \varphi)(\rho C_p)_{DW} + \varphi(\rho C_p)_{CuO/Cu} \quad (14-a)$$

$$(\rho C_p)_{hybrid} = (1 - \varphi_{CuO} - \varphi_{Cu})(\rho C_p)_{DW} + \varphi_{CuO}C_{pCuO} + \varphi_{Cu}C_{pCu} \quad (14-b)$$

Brinkman equation (Brinkman, 1952) can be applied to estimate the effective dynamic viscosity of the spherical-mono and spherical-hybrid nanofluids (Benkhedda et al., 2019):

$$(\mu)_{nf} = \frac{\mu_{DW}}{(1 - \varphi)^{2.5}} \quad (15-a)$$

$$(\mu)_{hybrid} = \frac{\mu_{DW}}{(1 - \varphi_{CuO} - \varphi_{Cu})^{2.5}} \quad (15-b)$$

Meanwhile, dynamic viscosity for Cylindrical-shaped, Platelets-shaped and Blades-shaped mono and hybrid nanofluids can be estimated from Eq. (16) (Timofeeva et al., 2009):

$$(\mu)_{nf} = \mu_{DW} \times (1 + A\varphi + B\varphi^2) \quad (16-a)$$

$$(\mu)_{hybrid} = \mu_{DW} \times (1 + A(\varphi_{CuO} + \varphi_{Cu}) + B(\varphi_{CuO} + \varphi_{Cu})^2) \quad (16-b)$$

Constant	Platelet-shaped	Blade-shaped	Cylinder-shaped
A	37.1	14.6	13.5
B	612.6	123.3	904.4

According to Ellahi et al. (2015), the effective thermal conductivity of the spherical-mono and spherical-hybrid nanofluids can be expressed as below (Benkhedda et al., 2019):

$$k_{nf} = k_{DW} \left(\frac{k_{CuO/Cu} + (m + 1)k_{DW}}{-(m + 1)\varphi(k_{DW} - k_{CuO/Cu})} \right) \quad (17-a)$$

Table 2. Sphericity (Ψ) and nanoparticle shape factor (m) used in Eq. (17).

Nanoparticle	Ψ	$m = 3/\Psi$
Spherical-shaped	1	3
Cylindrical-shaped	0.62	4.9
Platelets-shaped	0.82	5.7
Blades-shaped	0.36	8.6

$$k_{hybrid} = k_{DW} \left(\frac{\frac{\varphi_{CuO}k_{CuO} + \varphi_{Cu}k_{Cu}}{\varphi} + (m + 1)k_{DW}}{-(m + 1)\varphi \left(k_{DW} - \frac{\varphi_{CuO}k_{CuO} + \varphi_{Cu}k_{Cu}}{\varphi} \right)} \right) \quad (17-b)$$

As shown above, the Maxwell equation was used for spherical-mono and spherical-hybrid nanofluids in different volumetric percentages. Hamilton–Crosser modified the Maxwell model to estimate the thermal conductivity of Cylindrical-shaped, Platelets-shaped, and Blades-shaped mono and hybrid nanofluids. (m) is the shape factor was given by $(3/\Psi)$. (Ψ) refers to the sphericity of nanoparticles and its value for spherical nanoparticles is ($\Psi = 1$), which corresponds to a shape factor of ($m = 3$). The (m and Ψ) values are given in Table 2 for mono and hybrid nanofluids in different nanoparticle shapes.

3. Validation and verification of the numerical results

The grid independence test is carried out when configuring flat plate solar collectors using base fluid (DW) to verify the numerical results are reliable. As a result, the tested solar collector using water as a working fluid has five possible grids (462,000 elements, 612,600 elements, 697,800 elements, 773,400 elements, and 872,000 elements) are investigated under the parameters of 293 K and $Re = 500$. Five parameters are used for grid verifications: pressure drop, temperature difference (outlet – inlet), heat gain, collector efficiency, and surface temperature. Figure 2 shows that as the number of elements increases, the accuracy of the data collected increases. Due to its correctness and accuracy, grid number (5) with 872,000 elements is adopted for further processing the remaining tests in the current study.

Figure 3 illustrates the comparison of thermal efficiency between the current numerical results and the experimental data available from Verma et al. (2018) and (Verma et al., 2017). The medium dispersion (DW), three conventional nanofluids (MgO-DW, CuO-DW, and MWCNTs-DW), and two mixture nanofluids (MgO@MWCNTs-DW) and (CuO@MWCNTs-DW)

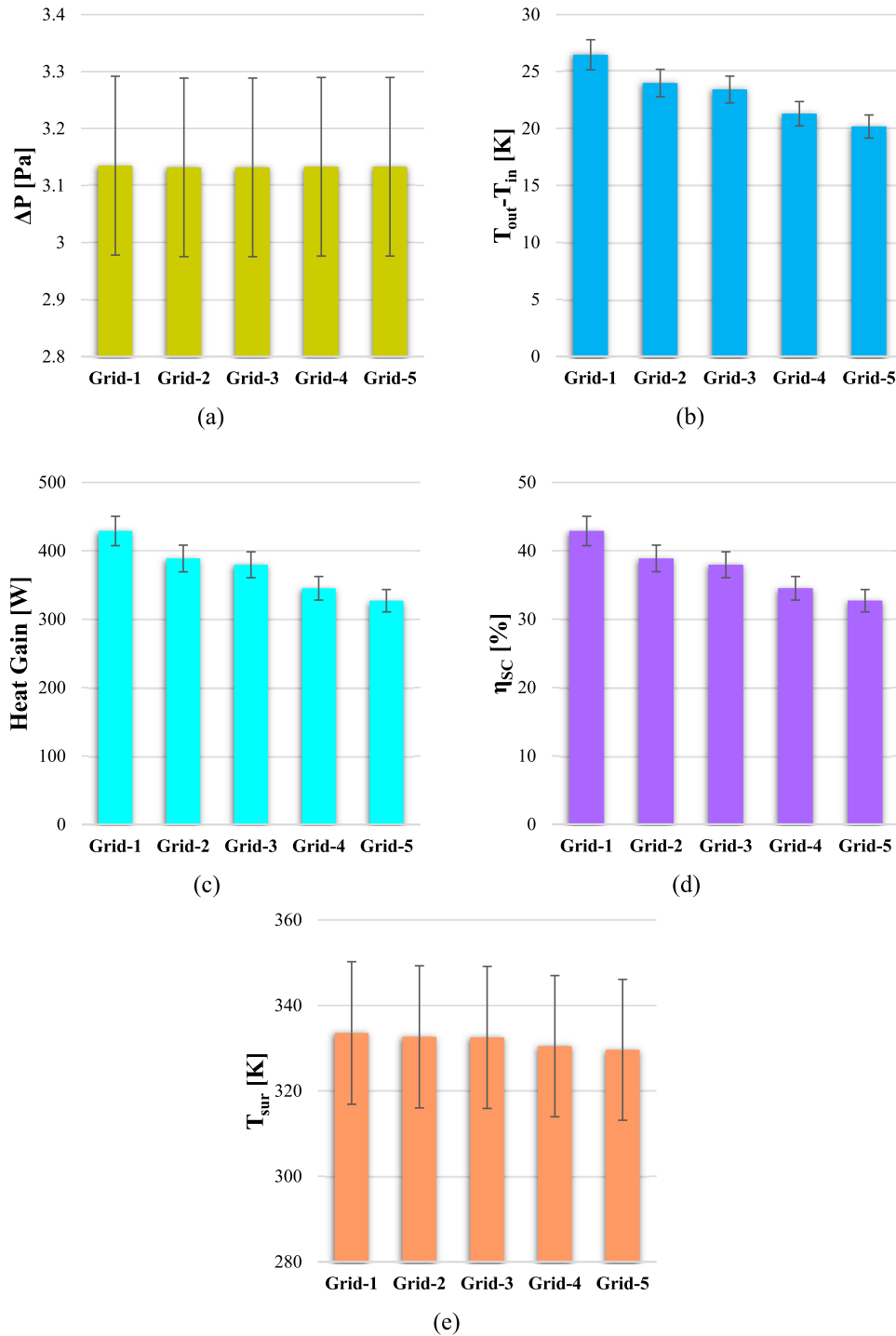


Figure 2. Grid independence test with different parameters; (a) pressure drop, (b) difference, (c) heat gain, (d) collector efficiency, (e) surface temperature, using DW with 293 K and $Re = 500$.

were properly considered at $T_a = 300$ K, $I = 800$ W/m², and 0.025 kg/s. The average error between the previous experimental and current numerical observations were $\pm 4.1\%$ for DW, $\pm 4.2\%$ for MgO-DW, $\pm 6.3\%$ for CuO/DW, $\pm 4.4\%$ for MWCNTs-DW, $\pm 5.8\%$ for MgO@MWCNTs-DW, and $\pm 4.6\%$ for CuO@MWCNTs-DW. The average errors between the experimental and numerical data can be caused by the simplifications

and assumptions applied in the simulation's cases on the one hand and the uncertainties of the measuring tools and devices in the experimental part on the other hand. Based on the findings, the CFD thermal model can be recommended to evaluate the energy performance of base fluids, single nanofluids, and mixture nanofluids under different simulation conditions.

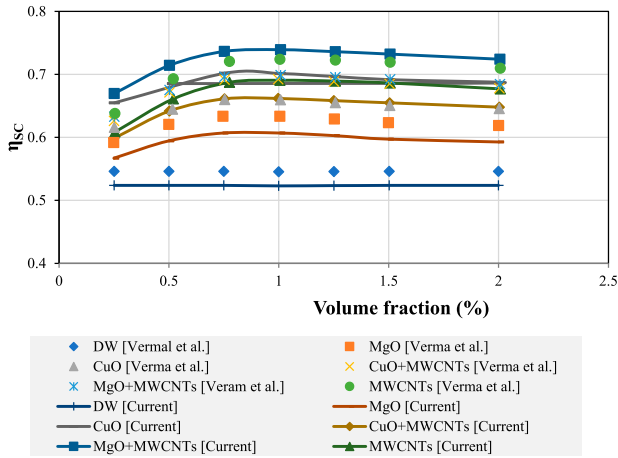


Figure 3. Validation approach for the current study and the previous experimental study from Verma et al. (Verma et al., 2018),(Verma et al., 2017).

4. Results and discussion

4.1. Property enhancement ratio (PER)

The maximum heat transfer condition was estimated using the ratio of dynamic viscosity (negative parameter) to thermal conductivity (positive parameter) of

nanofluids/base fluid. Eq. (18) describes the property enhancement ratio (PER). When (PER) is > 5, the mono/hybrid nanofluid doesn't enhance heat transfer performance, according to the analysis of (Abdolbaqi et al., 2017).

$$PER = \frac{\mu_r - 1}{k_r - 1} = \frac{k_{DW}(\mu_{nf} - \mu_{DW})}{\mu_{DW}(k_{nf} - k_{DW})} \quad (18)$$

The effect of PER was shown to be substantially influenced by changes in dynamic viscosity and thermal conductivity values. As a result, the PER showed in Figure 4 accurately anticipated the numerical conditions of heat enhancement for various mono and hybrid nanofluids on multiple shapes at different volumetric percentages. As per Figure 4, with 1 and 2 vol.%, Cu-DW-Platelets nanofluid showed higher with PER = 5.623 and 6.355, using 1volume% and 2 volume%, respectively. Meanwhile, with 3volume% and 4volume%, Cu-DW-Cylindrical and Cu-DW-Platelets nanofluids showed (5.773 and 7.072) and (6.986 and 7.773), respectively. In addition, CuO-DW in various volumetric percentages had the lowest PER values, as shown in Figure 4.

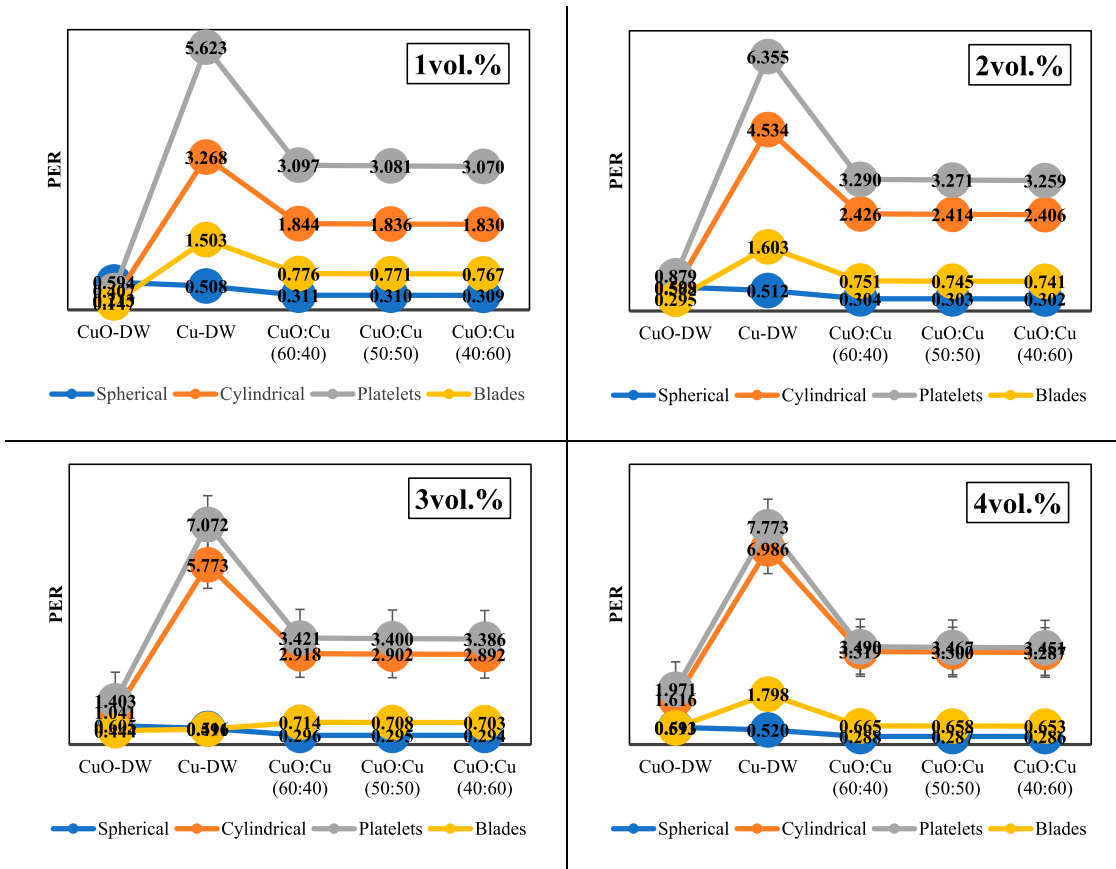


Figure 4. Property enhancement ratio (PER) of conventional and mixture nanofluids with different volumetric percentages and different nanoparticles geometries at 293 K.

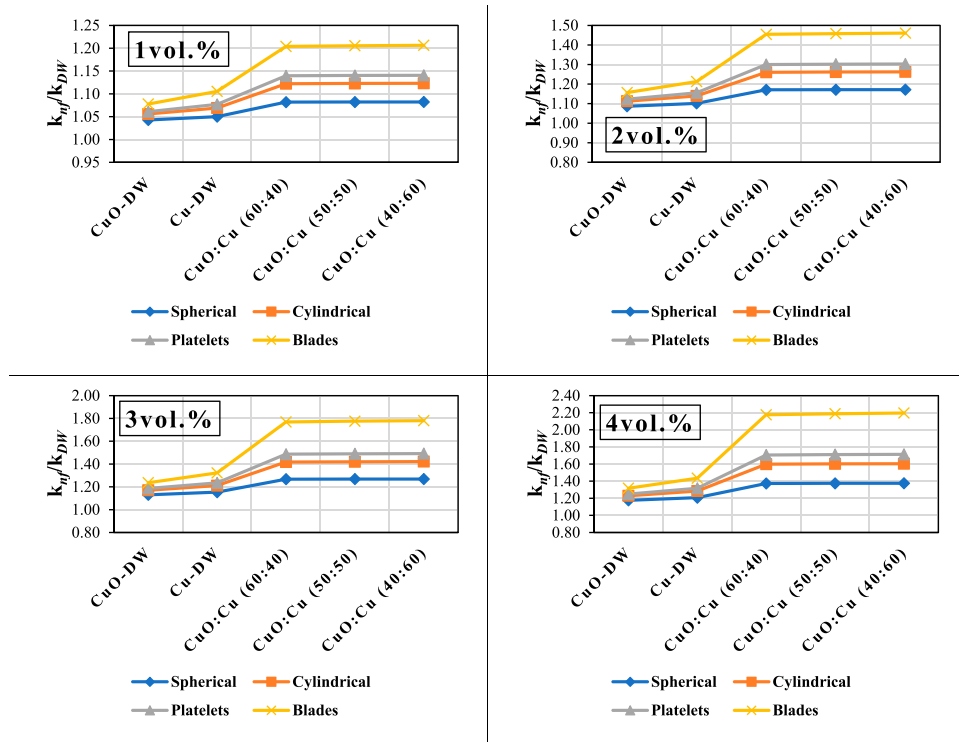


Figure 5. Thermal conductivity ratio of single and mixture nanofluids with different volumetric percentages and nanoparticles shapes at 293 K.

4.2. Thermal conductivity ratio

Thermal conductivity is the most intriguing property of nanofluids that has attracted the curiosity of researchers. Although this is a complicated and significant thermo-physical phenomenon, experimental studies and theories have failed to explain why hybrid nanofluids have high thermal conductivity. Figure 5 reveals the thermal conductivity ratio (k_{nf}/k_{DW}) of single and mixture nanofluids in different nanoparticle morphologies at 293 K. The thermal conductivity ratio (k_{nf}/k_{DW}) increased with increasing volumetric percentage, and this tendency was evident for all single and mixture nanofluids in various nanoparticle geometric shapes. CuO@Cu-Blades (60:40), CuO@Cu-Blades (50:50), and CuO@Cu-Blades (40:60) showed higher thermal conductivity ratios such as (1.204, 1.205, and 1.206), (1.454, 1.458 and 1.461), (1.769, 1.776 and 1.781) and (2.175, 2.188 and 2.197), respectively, for 1volume%, 2volume%, 3volume%, and 4volume%. They are adding additional Cu to the hybrid nanofluids slightly enhanced the thermal conductivity ratio. Cu-DW in various shapes showed minor increments over CuO-DW in different shapes compared to mono nanofluids with varying volumetric percentages. Moreover, in mono nanofluids, Blade-nanoparticles illustrated the best values, followed by Platelets-shaped, Cylindrical-shaped, and spherical-shaped, respectively. According to studies (Babar & Ali, 2019), (Gupta et al., 2018), (Yang et al.,

2020), as the surface-to-volume ratio of nanoparticles increases, so does their thermal conductivity. This is because nanomaterials with a larger specific surface area have better heat exchange capability and lower thermal resistance. Furthermore, according to a study, the shape of a nanoparticle has a real impact on its long-term stability (Chakraborty & Panigrahi, 2020). They concluded that blade-shaped particles sediment faster than platelet- and brick-shaped particles. In the suspended state, brick-shaped nanoparticles are highly stable. It can be concluded that the long-term stability of nanofluids is critical because the sedimentation process reduces the thermal properties of nanofluids.

4.3. Prandtl number (Pr)

The Prandtl number (Pr) is dimensionless and represents the ratio between the heat transfer fluids' momentum and heat transport. As a result, it evaluates the relationship between a fluid's momentum diffusivity and thermal diffusivity. Prandtl number (Pr) can be defined as follows:

$$Pr = \frac{\text{Momentum diffusivity}}{\text{Thermal diffusivity}} = \frac{\mu \times C_p}{k} \quad (19)$$

A high Pr-number (> 5) indicates that heat transfer via fluid momentum is preferable to thermal diffusion. In other words, a high Pr-number shows that heat transfer is more likely to occur through fluid momentum

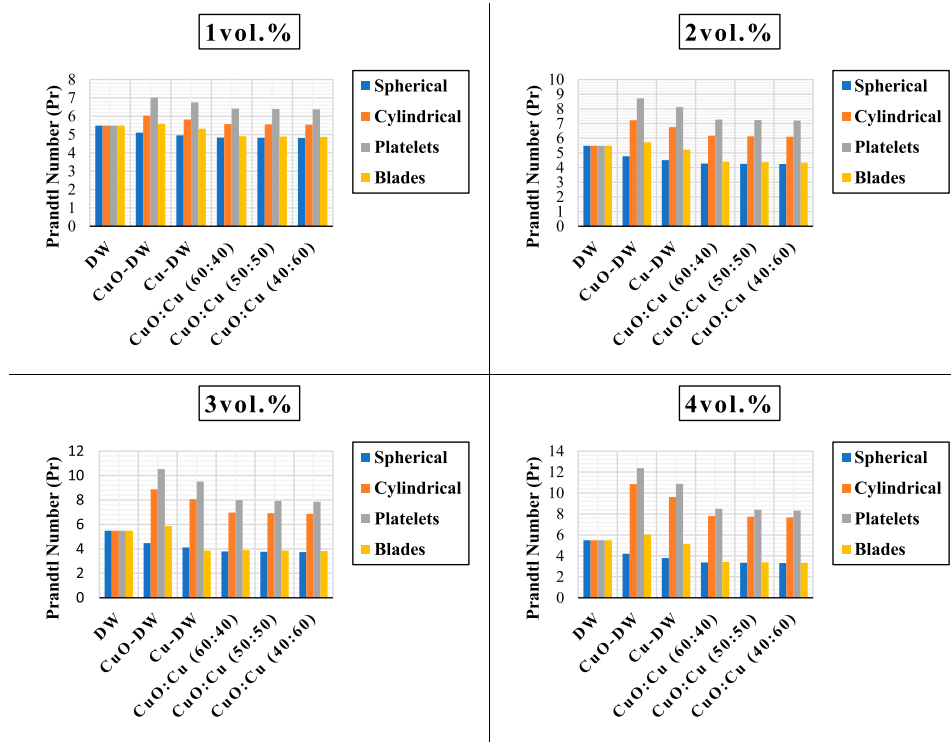


Figure 6. Prandtl number of single and mixture nanofluids with different volumetric percentages and nanoparticles shapes at 293 K.

rather than fluid conduction. According to Figure 6, the Platelets-shaped had higher Pr-number values than others for all mono and hybrid nanofluids at different volumetric percentages. CuO/DW-Platelets nanofluids presented the best values for Pr-number followed by Cu/DW-Platelets, 60%-CuO@40%-Cu/DW-Platelets, 50%-CuO@50%-Cu/DW-Platelets and 40%-CuO@60%-Cu/DW-Platelets such as (7.009, 6.749, 6.413, 6.394 and 6.376), (8.717, 8.115, 7.276, 7.236 and 7.198), (10.526, 9.506, 7.987, 7.922 and 7.863) and (12.377, 10.874, 8.494, 8.406 and 8.325) for 1 volume%, 2, 3 and 4 volume%, respectively. As per Eq. (19), The Pr-numbers are affected by three major thermal-physical properties, which are as $(\frac{\mu \times C_p}{k})$. Eq. (16) shows that the dynamic viscosity of different mono and hybrid nanofluids for the same nanoparticle shape is the same value. Higher specific heat and lower thermal conductivity values will result in a higher Pr-number. Under the conditions of 293 K and 1 volume%, the values for specific heat and thermal conductivity values as follows (3956.863 and 0.6387 W/m-K), (3867.085 J/kg-K and 0.6483 W/m-K), (3887.964 J/kg-K and 0.6860 W/m-K), (3879.062 J/kg-K and 0.6865 W/m-K) and (3870.201 J/kg-K and 0.6868 W/m-K) for CuO/DW-Platelets, Cu/DW-Platelets, 60%-CuO@40%-Cu/DW-Platelets, 50%-CuO@50%-Cu/DW-Platelets, and 40%-CuO@60%-Cu/DW-Platelets, respectively. In general, nanoparticles with non-spherical shapes that contained nanofluid displayed higher

viscosities than those with spherical shapes. Researchers attributed the higher viscosity of the nanofluid to the larger surface area of the non-spherical nanoparticle (Khan & Valan Arasu, 2019). Overall, particles with non-spherical shapes had higher enhancements in thermal conductivity. Moreover, The nanoparticles may have a higher value of specific heat capacity due to their large specific surface area compared to the base fluids, which contributes to the enhancement of the specific heat capacity of nanofluids (Munyalo & Zhang, 2018). To conclude, the difference in thermo-physical properties could be attributed to a difference in effective aggregation radius between the two nanoparticle shapes under consideration (Khan & Valan Arasu, 2019).

4.4. Mono and hybrid nanofluids in different shapes

In this section, six different parameters are thoroughly discussed, including pressure drop (ΔP), difference temperature (Tout-Tin), Surface heat transfer coefficient, energy gain (Qin), solar collector efficiency (η_{SC}), and flat plate surface temperature (Tsur) for base fluid (DW) and different mono/hybrid nanofluids in various morphologies and different mixing ratios under testing conditions of 1 volume%, 293 K, and $500 \leq Re \leq 1900$.

Figure 7 depicts the pressure drop of base fluid (DW) and different mono/hybrid nanofluids in various shapes and different mixing ratios under the testing conditions

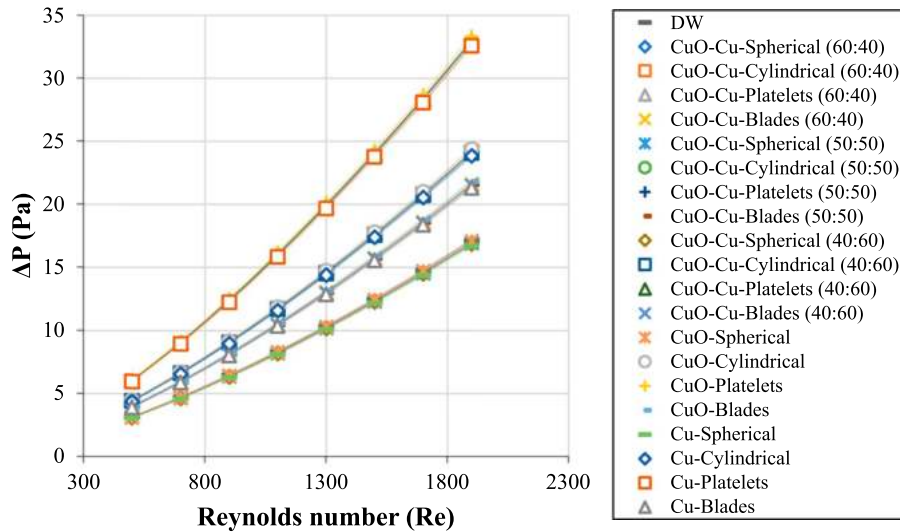


Figure 7. Pressure drop of single and mixture nanofluids with different Reynolds numbers and nanoparticles shapes at 293 K and 1volume%.

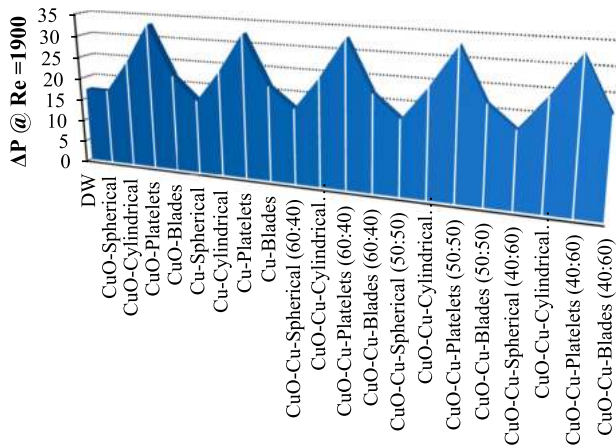


Figure 8. Pressure drop of single and mixture nanofluids with different nanoparticles shapes at 293 K, 1volume% and $Re = 1900$.

of 1volume%, 293 K, and $500 \leq Re \leq 1900$. Meanwhile, Figure 8 depicts the pressure drop of the base fluid and mono/hybrid nanofluids with various nanoparticle shapes at 293 K, 1volume%, and $Re = 1900$. The pressure decreases as the Reynolds number increase for base fluid and nanofluids in different shapes. As stated by previous studies (Ahmed et al., 2022; Tao et al., 2022), the density value of other solid nanoparticles is crucial for nanofluids' increased pressure drop and friction factor. Also, the pressure loss in thermal applications is directly proportional to the dynamic viscosity of the working fluid. This increase in the dynamic viscosity of nanofluids causes an unfavorable increase in the pumping power. As a result, designing a solar collector for efficient heat transfer and low pumping power is critical for energy savings. It may result in significant errors when evaluating the overall performance of nanofluids in various thermal science

and engineering applications. According to Figures 7 and 8, base fluid exhibits more significant pressure loss than spherical-mono and spherical-hybrid nanofluids. Meanwhile, the pressure loss values for Platelets-mono and Platelets-hybrid nanofluids are higher than those for Cylindrical and Blades. The variations in pressure drop when using mono and hybrid nanofluids with different shapes can be attributed to Pr number values (Figure 6). The Pr-number for spherical-mono and spherical-hybrid nanofluids is lower than that of base fluid (DW). Meanwhile, for pressure loss, Platelets-mono and Platelets-hybrid nanofluids have the highest Pr-number, followed by Cylindrical and Blades. Furthermore, pressure drops are more significant when using CuO-Platelets nanofluid, followed by CuO-Cu-Platelets (60:40), CuO-Cu-Platelets (50:50), CuO-Cu-Platelets (40:60), and Cu-Platelets. The variations in the pressure drop values using different mono and hybrid nanofluids in the shape of Platelets can be attributed to the value of nanofluid velocity, which is 0.1632, 0.1618, 0.1614, 0.1610, and 0.1596 m/s for CuO- Platelets, CuO-Cu-Platelets (60:40), CuO-Cu-Platelets (50:50), CuO-Cu-Platelets (40:60) and Cu-Platelets, respectively. Appendix (A) compares the velocity profiles of different mono and hybrid nanofluids in different morphologies at 1 vol.% and $Re = 1900$.

The outlet temperature (T_{out}) is an essential consideration for the FPSC's thermal performance. Figure 9 shows the outlet-temperature – inlet-temperature ($T_{out} - T_{in}$) of dispersion medium (DW) and different single/mixture nanofluids in various nanoparticles shapes and various mixing ratios under the simulation conditions of 1volume%, 293 K and $500 \leq Re \leq 1900$. Meanwhile, Figure 10 illustrates the ($T_{out} - T_{in}$) of dispersion medium and single/mixture nanofluids with

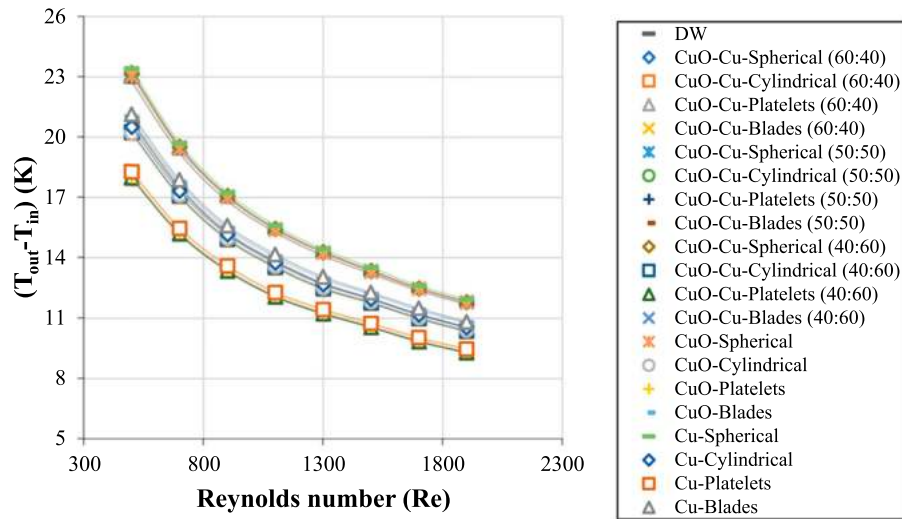


Figure 9. Temperature variation of single and mixture nanofluids with various Reynolds numbers and different nanoparticles shapes at 293 K and 1volume%.

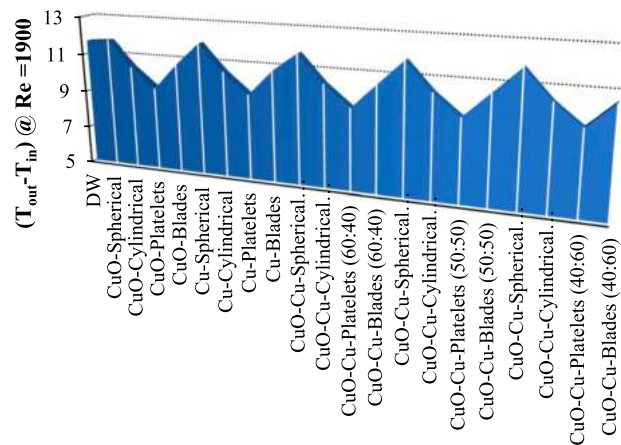


Figure 10. Temperature difference of mono and hybrid nanofluids with various nanoparticles structures at 293 K, 1volume%, and $Re = 1900$.

various nanoparticles shapes at 293 K, 1volume%, and $Re = 1900$. The output temperature drops as the Reynolds number (velocity) of the dispersion medium and single/mixture nanofluids rises owing to the decreased fluid surface contact time, which influences the efficiency enhancement (Choudhary et al., 2020). Due to the minimum thermal conductivity increase, spherical-shaped single and mixture nanofluids have a more significant outlet/temperature – inlet/temperature ($T_{out}-T_{in}$) than other morphologies under the same testing circumstances, as demonstrated in Figure 5. Meanwhile, Platelets-shaped single and mixture nanofluids show the lower values for temperature difference ($T_{out}-T_{in}$), followed by Cylindrical-shaped and Blades-shaped nanofluids. Furthermore, CuO-Cu-Platelets (60:40) display the lowest ($T_{out}-T_{in}$) values, followed by CuO-Cu-Platelets

(50:50), CuO-Cu-Platelets (40:60), CuO-Platelets and Cu-Platelets, in that order. The variations in ($T_{out}-T_{in}$) values using different single and mixture nanofluids in the Platelets-shaped can be credited the value of nanofluid velocity as follows; 0.1632, 0.1618, 0.1614, 0.1610 and 0.1596 m/s for CuO- Platelets, CuO-Cu-Platelets (60:40), CuO-Cu-Platelets (50:50), CuO-Cu-Platelets (40:60) and Cu-Platelets, respectively. It is worth mentioning that a lesser temperature difference is not recommended in thermal science and engineering applications. Because single/mixture nanofluids function in a closed piping loop in the solar collector, the low temperature will not transfer heat through headers and risers tubes. However, it is possible to compensate by increasing the number of fluid flows in the thermal system, which may raise the pumping power cost. The difference between the fluid outlet and fluid inlet temperatures at a low Reynolds number becomes enormous as the circulating fluid spends more time in the collector system, encouraging heat losses and lowering thermal performance. In conclusion, volumetric flow rates that were neither too high nor excessively low were confirmed to be suitable (Choudhary et al., 2020).

The surface temperature of the thin-plate is higher in the solar collector system because the surface absorbs a wide range of the sun's heat flux. Figure 11 shows the surface temperature of base fluid (DW) and various mono/hybrid nanofluids in multiple structures and different mixing ratios under the testing conditions of 1volume%, 293 K, and $500 \leq Re \leq 1900$. Meanwhile, Figure 12 demonstrates the surface temperature of the base fluid and mono/hybrid nanofluids with various nanoparticle shapes at 293 K, 1volume%, and $Re = 1900$. The surface temperature of the base fluid and

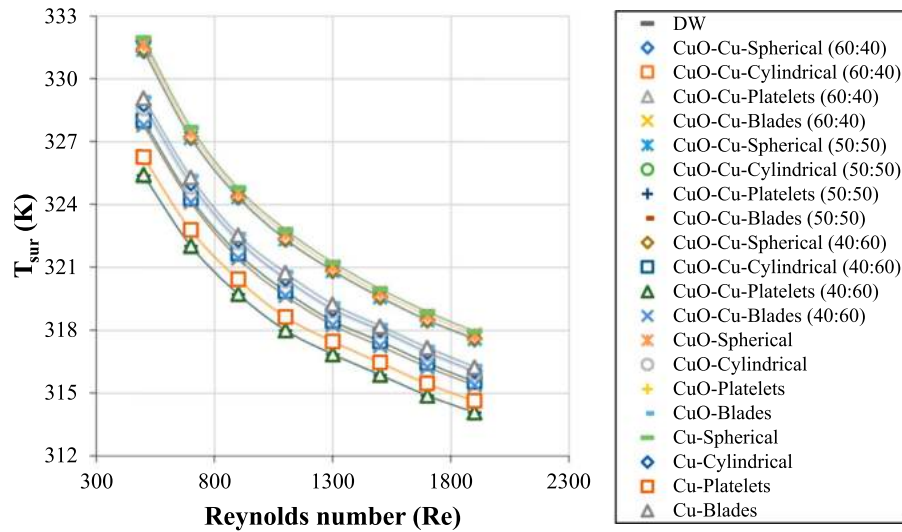


Figure 11. Surface temperature of single and mixture nanofluids with various Reynolds numbers and nanoparticles morphologies at 293 K and 1volume%.

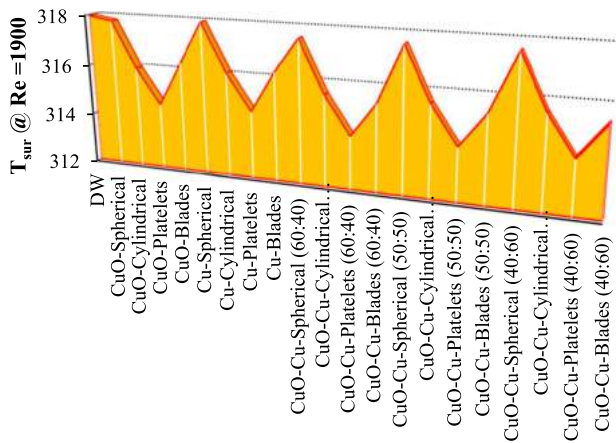


Figure 12. Surface temperature of single and mixture nanofluids with various nanoparticles morphologies at 293 K, 1volume%, and $Re = 1900$.

mono/hybrid nanofluids in different shapes decreases as the Reynolds number increases. Except for Cu-Spherical, which showed slightly higher temperatures than the base fluid, the surface temperature of Spherical-shaped mono and hybrid nanofluids decreased slightly compared to DW. At $Re = 1900$, CuO-Cu-Platelets (60:40) shows the lowest surface temperature (314.065 K), followed by CuO-Cu-Platelets (50:50) with (314.074 K) and CuO-Cu-Platelets (40:60) with (314.081 K). Furthermore, cylindrical-shaped mono and hybrid nanofluids have the lowest surface temperatures, followed by blade-shaped nanofluids. The higher thermal performance of mono/hybrid nanofluids was attributable to a decline in circulation temperature following a rise in thermal conductivity in the heat transfer fluid, which reduced the temperature gradient between the flat-tube wall and the bulk fluid contained in the solar collector system

(Bezaatpour & Rostamzadeh, 2021). Therefore, lowering the thin-flat plate's maximum temperature is essential for preventing such enormous energy inefficiency. The thermal system performs better in heat transfer mechanisms with the thin thermal boundary layers, which induced greater velocities (mass/volume flow rates), increasing thermal conductivity and lowering thermal resistance between the flowing single/mixture nanofluid and the temperature of the collector's internal wall surface (Xiong et al., 2021).

Figure 13 depicts the heat gain of base fluid (DW) and other single/mixture nanofluids in various geometries and mixing ratios under 1volume%, 293 K, and $500 \leq Re \leq 1900$ as testing conditions. Meanwhile, at 293 K, 1volume%, and $Re = 1900$, Figure 14 shows the Heat Gain of the base fluid and single/mixture nanofluids with various nanoparticle morphologies. As shown below, heat gain (Q_{in}) increases as the Reynolds number increases for base fluid and single/mixture nanofluids in different shapes due to the mass flow rate values (Eq. 12). The spherical-shaped single and mixture nanofluids demonstrate less energy performance than base fluid because the higher temperature difference ($T_{out}-T_{in}$) for spherical-nanofluids. Also, Platelets-shaped single and combination nanofluids demonstrate higher values for energy gain followed by Cylindrical-shaped and Blades-shaped due to the values of Pr-number. Moreover, CuO-Platelets reports the best energy enhancement, followed by Cu-Platelets, CuO-Cu-Platelets (60:40), CuO-Cu-Platelets (50:50), and CuO-Cu-Platelets (40:60), respectively. Platelets-shaped single and mixture nanofluids have the same dynamic viscosity, with temperature differences playing the essential effect (Bretado-de los Rios et al., 2021).

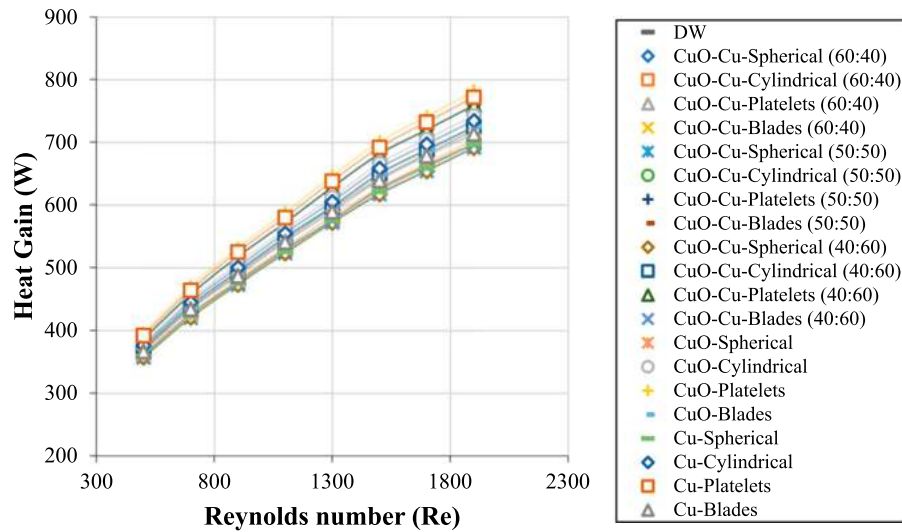


Figure 13. Heat gain of single and mixture nanofluids versus different Reynolds numbers and nanoparticles shapes at 293 K and 1volume%.

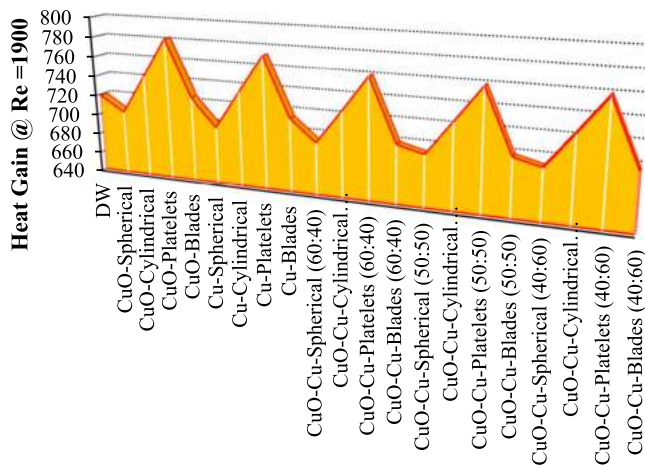


Figure 14. Heat gain of single and mixture nanofluids with various nanoparticles shapes at 293 K, 1volume% and $Re = 1900$.

Figure 15 depicts the Surface heat transfer coefficient of base fluid (DW) and another single/mixture nanofluids in various geometries and mixing ratios under 1volume%, 293 K, and $500 \leq Re \leq 1900$ as testing conditions. Meanwhile, at 293 K, 1volume%, and $Re = 1900$, Figure 16 shows the Surface heat transfer coefficient of the base fluid and single/mixture nanofluids with various nanoparticle morphologies. As shown below, heat transfer increases as the Reynolds number increases for base fluid and single/mixture nanofluids in different shapes due to the mass flow rate values (Eq. 12). The spherical-shaped single and mixture nanofluids demonstrate less heat transfer performance such as (CuO-Cu-Spherical (60:40) with 1.5%, CuO-Cu-Spherical (50:50) with 1.4%, CuO-Cu-Spherical (40:60) with 1.34%, CuO-Spherical with 0.625 and Cu-Spherical with 0.14%) because the higher temperature difference (Tout-Tin) for

spherical-nanofluids. Also, Platelets-shaped mixture and single nanofluids demonstrate higher values for heat transfer, such as (CuO-Cu-Platelets (60:40) with 15.13%, CuO-Cu-Platelets (50:50) with 15.09%, CuO-Cu-Platelets (40:60) with 15.05%, CuO-Platelets with 12.78% and Cu-Platelets with 12.55%) followed by Blades-shaped and Cylindrical-shaped as mixture nanofluids. In general, the mixing ratio of (60:40) slightly enhances the heat transfer than the other ratios of (50:50) and (40:60). According to earlier research, nanofluids with higher thermal conductivity than their base fluids frequently have higher convective heat transfer coefficients in both laminar and turbulent regimes (Alawi et al., 2020).

Figure 17 shows the collector efficiency of dispersion medium (DW) and different single/mixture nanofluids in different shapes and different mixing ratios under the simulation conditions of 1volume%, 293 K, and $500 \leq Re \leq 1900$. Meanwhile, Figure 18 illustrates the solar collector efficiency of DW and single/mixture nanofluids with different nanoparticle structures at 293 K, 1 vol.%, and $Re = 1900$. One of the most important scientific facts that, when the fluid Re-number of HTFs rises, the thermal resistance between the working fluid and the flat-tube wall decreases (Genc et al., 2018). In other words, collector efficiency improves as the mass flow rate increases regardless of the type of heat transfer fluids (DW or single/mixture nanofluids). In this study, the solar collector efficiency of the spherical-shaped single and combination nanofluids is lower than DW. Also, Platelets-shaped single and mixture nanofluids have higher collector effectiveness than Cylindrical-shaped and Blades-shaped nanofluids. In specific, CuO-Platelets have the highest solar collector performance, followed by Cu-Platelets, CuO@Cu-Platelets (60:40),

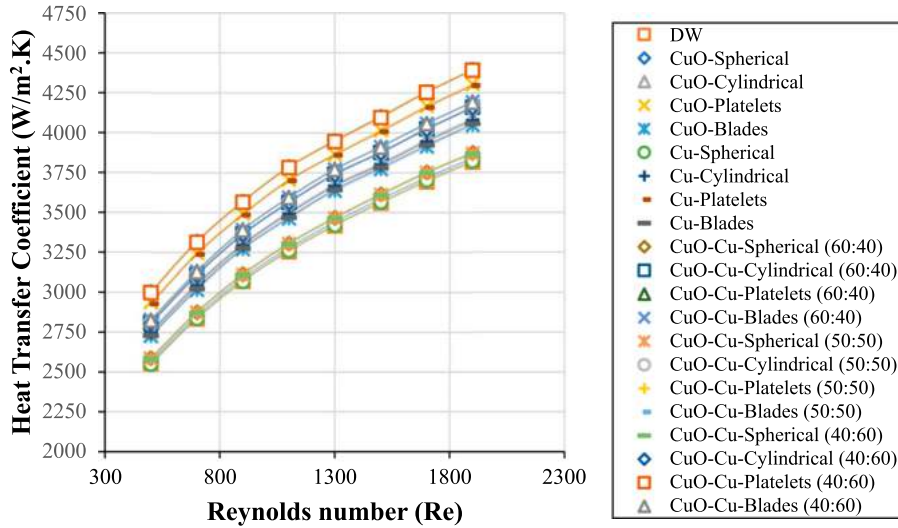


Figure 15. Surface heat transfer coefficient of mono and hybrid nanofluids with various Reynolds numbers and nanoparticles shapes at 293 K and 1volume%.

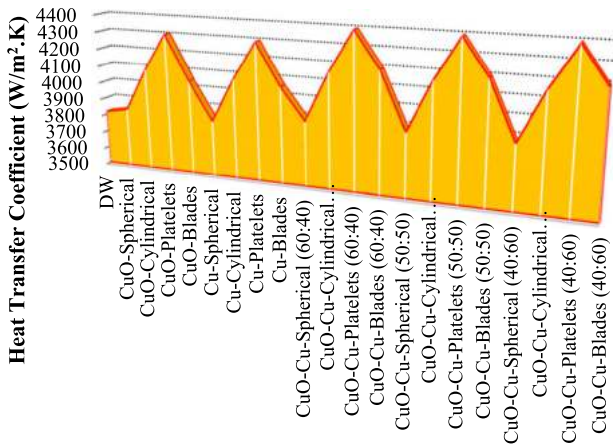


Figure 16. Surface heat transfer coefficient of single and mixture nanofluids with various nanoparticles shapes at 293 K, 1volume% and $Re = 1900$.

CuO@Cu-Platelets (50:50), and CuO@Cu-Platelets (40:60). In this regard, the Brownian motion of solid nanoparticles played the most critical role in this increase since the current problem was solved via forced flow. It's worth mentioning that forced flow increased the random motion of the solid nanoparticles, which increased the collision between working fluid molecules and nanomaterials. The convective heat transfer and collector efficiency improved accordingly (Farajzadeh et al., 2018). The enhanced thermal performance can be attributed to the increased thermal conductivity of single and mixture nanofluids in various nanoparticle morphologies, as demonstrated in both laminar and turbulent flows applications (Sarsam et al., 2020a),(Eltaweel et al., 2021). The increased thermal conductivity of the single/mixture nanofluids and the decrease in thermal

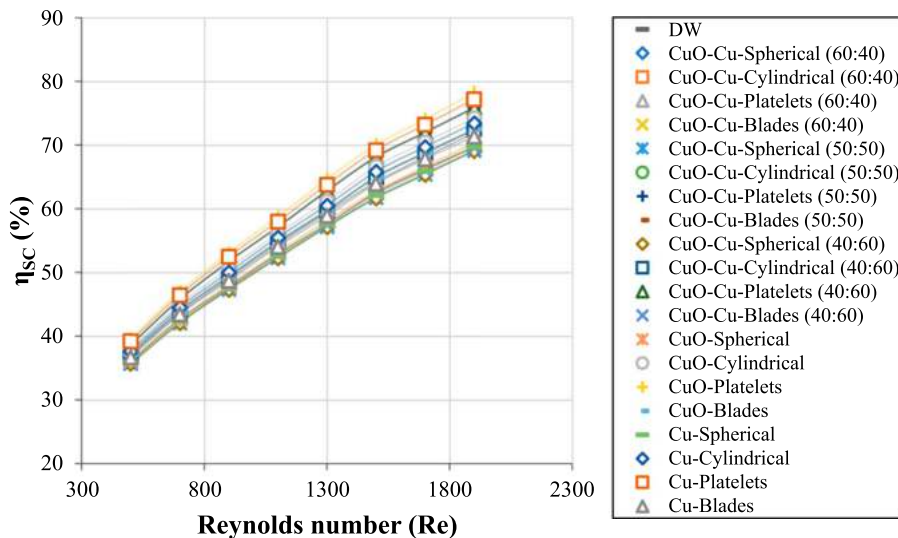


Figure 17. Solar collector efficiency of mono and hybrid nanofluids with various Reynolds numbers and nanoparticles shapes at 293 K and 1volume%.

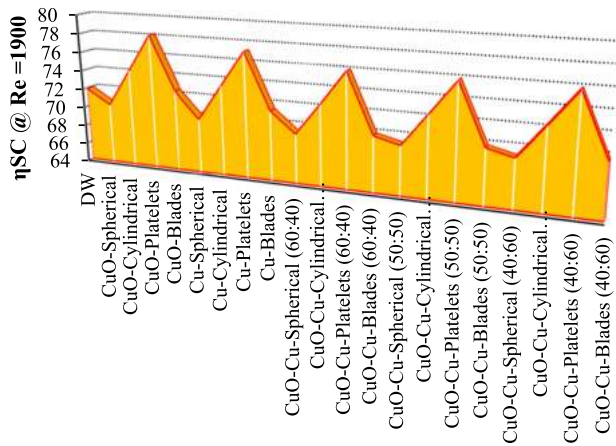


Figure 18. Solar collector efficiency of single and mixture nanofluids with various nanoparticles shapes at 293 K, 1 volume% and $Re = 1900$.

resistance between the working fluid and the inner wall of the riser flat-tube are mainly responsible for the improved solar collector performance. Single and mixture nanofluids produce thin thermal boundary thicknesses in various morphologies (Akram et al., 2021).

5. Size reduction and cost analysis

The solar collector efficiency (η_{SC}) as described in (Eq. 12) for DW and mono/hybrid nanofluids in various shapes improves with increasing Reynolds numbers (velocity) and volumetric nanoparticle percentages. The collector efficiency of mono/hybrid nanofluids is higher than DW in the collector with the same collector surface area and input energy (Q_{in}). As a result, the increased solar collector efficiency using different nanofluids translates into the potential size reduction of the solar collector's area (Sundar et al., 2020). As shown in Figure 19, the maximum area reduction is achieved by using CuO-Platelets with (25.60%), Cu-Platelets with (22.32%), CuO-Cu-Platelets with (60:40) (16.02%), CuO-Cu-Platelets (50:50) with (15.80%) and CuO-Cu-Platelets (40:60) with (15.51%). Moreover, cylindrical-shaped nanofluids show the possible size reduction of the solar collector's area such as CuO-Cylindrical with (21.95%), Cu-Cylindrical with (18.70%), CuO@Cu-Cylindrical (60:40) with (13.31%), CuO@Cu-Cylindrical (50:50) with (13.08%) and CuO@Cu-Cylindrical (40:60) with (12.79%). To compensate for the heat loss, spherical-shaped nanofluids require a collector that is greater than the current such as CuO-Cu-Spherical (40:60) with (16.69%), CuO-Cu-Spherical (50:50) with (16.32%), CuO-Cu-Spherical (60:40) with (15.95%), Cu-Spherical with (12.34%) and CuO-Spherical with (8.61%). Meanwhile, Blades-shaped nanofluids exhibit inconsistent

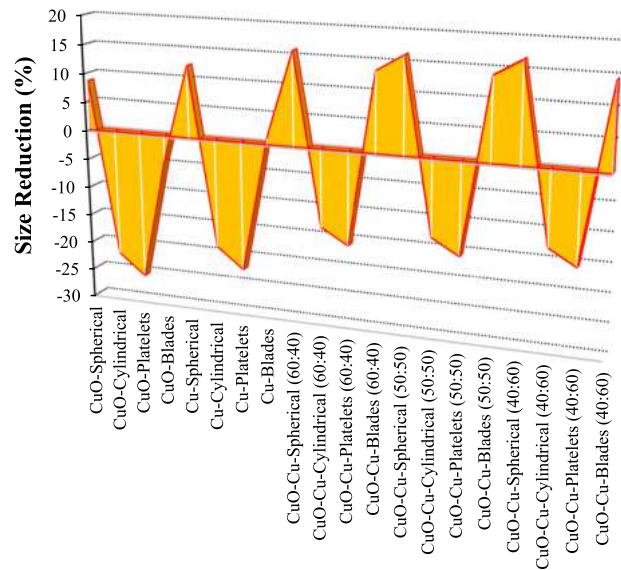


Figure 19. Size reduction of a collector using various mono/hybrid nanofluids at $Re = 1900$ and 4 volume%.

performance when the collection size is reduced or increased.

The total cost estimation is determined based on the collector's cost, independent costs and nanoparticles cost under the conditions of different-shaped single and mixture nanofluids in different mixing quantities at 293 K, 4 volume%, and $Re = 1900$. The cost of a single water-based collector and the independent (system and setup) are estimated as USD 250.60 and USD 771.42 as per the study (L. H. Kumar et al., 2021), which is decreased and increased based on the values of energy efficiency and size reduction as shown in Figure 20. Meanwhile, the cost of nanomaterials were taken from Sigma-Aldrich (M) Sdn Bhd. CuO-Platelets accomplish the best cost savings of a single flat plate collector with (USD 186.45) followed by Cu-Platelets with (USD 194.66), CuO-Cylindrical with (USD

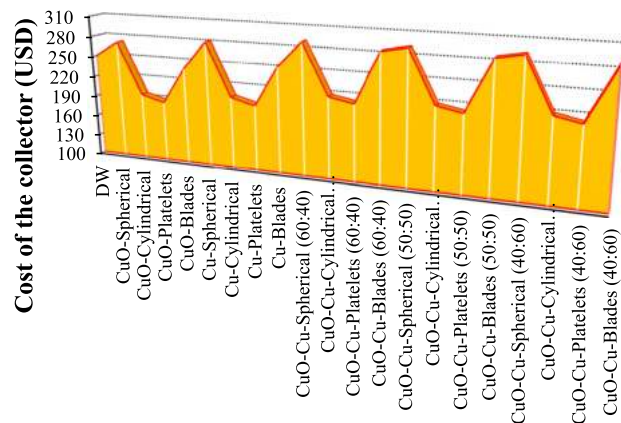


Figure 20. Cost estimation using different mono/hybrid nanofluids at $Re = 1900$ and 4 volume%.

195.59), Cu-Cylindrical with (USD 203.74), CuO@Cu-Platelets (60:40) with (USD 210.45), CuO@Cu-Platelets (50:50) with (USD 211), CuO@Cu-Platelets (40:60) with (USD 211.73), CuO@Cu-Cylindrical (60:40) with (USD 217.24), CuO@Cu-Cylindrical (50:50) with (USD 217.82) and CuO@Cu-Cylindrical (40:60) with (USD 218.55). Meanwhile, the cost of single solar collector for spherical-shaped and blades-shaped nanofluids increases such as CuO@Cu-Spherical (60:40) with (USD 290.57), CuO@Cu-Spherical (50:50) with (USD 291.50), CuO@Cu-Spherical (40:60) with (USD 292.42) and CuO@Cu-Blades (60:40) with (USD 284.55), CuO@Cu-Blades (50:50) with (USD 285.61), CuO@Cu-Blades (40:60) with (USD 286.73).

6. Conclusions

The thermal system of a flat plate solar collector made of a thin absorber and a flat tube was numerically modeled using various mono and hybrid nanofluids in multiple morphologies and mixing ratios. At 293 K, the thermo-physical properties of single and mixture nanofluids were estimated using a set of equations and empirical correlations. Several thermal and economic considerations were carried out to understand further the performance of individual and nanocomposites in solar collector applications. The following is a summary of the main findings:

- (i) Higher thermal conductivity ratio with 1.206, 1.205 and 1.204 were found in Blades-CuO@Cu (40:60), Blades-CuO@Cu (50:50), and Blades-CuO@Cu (60:40), respectively at 1volume%.
- (ii) CuO-DW-Platelets and Cu-DW-Platelets showed a higher Pr-number with 7.009 and 6.749 at 1volume%.
- (iii) Only Cu-DW-Platelets showed $PER > 5$ with (5.623) at 1volume%. Meanwhile, Cu-DW-Platelets and Cu-DW-Cylindrical demonstrated the same behavior when the volumetric percentage was increased to 4%.
- (iv) Platelets nanostructured fluids had higher pressure drop values, such as CuO-Platelets with (33.312 Pa), Cu-Platelets with (32.558 Pa), CuO@Cu-Platelets (60:40) with (33.006 Pa), CuO@Cu-Platelets (50:50) with (32.931 Pa) and CuO@Cu-Platelets (40:60) with (32.855 Pa), respectively at 1volume% and $Re = 1900$.
- (v) Cu-Spherical nanofluid was used to achieve a higher outlet–inlet temperature difference (Tout-Tin). Meanwhile, the lower (Tout-Tin) was reported by CuO@Cu-Platelets (60:40), CuO@Cu-Platelets (50:50), and CuO@Cu-Platelets (40:60) at 1volume% and $Re = 1900$.

- (vi) At 1volume% and $Re = 1900$, the CuO@Cu-Platelets (60:40), CuO@Cu-Platelets (50:50), and CuO@Cu-Platelets (40:60) enhanced the heat transfer by about 15.13%, 15.09% and 15.05%, respectively. Followed by CuO-Platelets and Cu-Platelets with 12.78% and 12.55%, respectively.
- (vii) CuO-Platelets reported better thermal enhancement with (8.761%) followed by Cu-Platelets with (7.355%), CuO@Cu-Platelets (60:40) with (5.666%), CuO@Cu-Platelets (50:50) with (5.544%) and CuO@Cu-Platelets (40:60) with (5.534%) at 1volume% and $Re = 1900$.
- (viii) The solar collector size was reduced by 25.60% using CuO-Platelets. Meanwhile, CuO@Cu-Spherical (40:60) required a bigger solar size with 16.69% at 4volume% and $Re = 1900$.
- (ix) The collector's cost was reduced to USD 186.45 using CuO-Platelets nanofluid. Meanwhile, the price increased to USD 292.42 using CuO@Cu-Spherical (40:60) at 4 vol.% and $Re = 1900$.
- (x) The total cost of CuO-Cu-Platelets (60:40), CuO-Cu-Platelets (50:50), and CuO-Cu-Platelets (40:60) were USD 994.82, USD 996.18, and USD 1004.52, respectively.

Disclosure statement

No potential conflict of interest was reported by the author(s).

ORCID

Nadhir Al-Ansari  <http://orcid.org/0000-0002-6790-2653>
Zaher Mundher Yaseen  <https://orcid.org/0000-0003-3647-7137>

References

- Abdolbaqi, M. K., Mamat, R., Sidik, N. A. C., Azmi, W. H., & Selvakumar, P. (2017). Experimental investigation and development of new correlations for heat transfer enhancement and friction factor of BioGlycol/water based TiO₂ nanofluids in flat tubes. *International Journal of Heat and Mass Transfer*, 108, 1026–1035. <https://doi.org/10.1016/j.ijheatmass-transfer.2016.12.024>
- Ahmed, W., Sidik, N. A. C., Mehmood, S., Alam, M. W., Fayaz, H., Hussain, M. I., Alawi, O. A., Ahmed, S. M., Shah, S. N. A., & Kazi, S. N. (2022). Effects of thermo-physical, hydrodynamics and thermal characteristics of well stable metallic nanofluids on energy transportation. *Journal of Thermal Analysis and Calorimetry*, 147(23), 13879–13900. <https://doi.org/10.1007/s10973-022-11696-8>
- Akram, N., Montazer, E., Kazi, S. N., Soudagar, M. E. M., Ahmed, W., Zubir, M. N. M., Afzal, A., Muhammad, M. R., Ali, H. M., Márquez, F. P. G., & Sarsam, W. S. (2021). Experimental investigations of the performance of a flat-plate solar collector using carbon and metal oxides based nanofluids. *Energy*, 120452. <https://doi.org/10.1016/j.energy.2021.120452>

- Alawi, O. A., Kamar, H. M., Mallah, A. R., Mohammed, H. A., Kazi, S. N., Sidik, N. A. C., & Najafi, G. (2020). Nanofluids for flat plate solar collectors: Fundamentals and applications. *Journal of Cleaner Production*, 125725. <https://doi.org/10.1016/j.jclepro.2020.125725>
- Babar, H., & Ali, H. M. (2019). Towards hybrid nanofluids: Preparation, thermophysical properties, applications, and challenges. *Journal of Molecular Liquids*, 598–633. <https://doi.org/10.1016/j.molliq.2019.02.102>
- Benkhedda, M., Boufendi, T., Tayebi, T., & Chamkha, A. J. (2019). Convective heat transfer performance of hybrid nanofluid in a horizontal pipe considering nanoparticles shapes effect. *Journal of Thermal Analysis and Calorimetry*, 140(1), 411–425. <https://doi.org/10.1007/s10973-019-08836-y>
- Bezaatpour, M., & Rostamzadeh, H. (2021). Simultaneous energy storage enhancement and pressure drop reduction in flat plate solar collectors using rotary pipes with nanofluid. *Energy and Buildings*, 239, 110855. <https://doi.org/10.1016/j.enbuild.2021.110855>
- Bhattad, A., Sarkar, J., & Ghosh, P. (2019). Experimentation on effect of particle ratio on hydrothermal performance of plate heat exchanger using hybrid nanofluid. *Applied Thermal Engineering*, 162, 114309. <https://doi.org/10.1016/j.applthermaleng.2019.114309>
- Bretado-de los Rios, M. S., Rivera-Solorio, C. I., & Nigam, K. D. P. (2021). An overview of sustainability of heat exchangers and solar thermal applications with nanofluids: A review. *Renewable and Sustainable Energy Reviews*, 142, 110855. <https://doi.org/10.1016/j.rser.2021.110855>
- Brinkman, H. C. (1952). The viscosity of concentrated suspensions and solutions. *The Journal of Chemical Physics*, 20(4), 571. <https://doi.org/10.1063/1.1700493>
- Chakraborty, S., & Panigrahi, P. K. (2020). Stability of nanofluid: A review. *Applied Thermal Engineering*, 174, 115259. <https://doi.org/10.1016/j.applthermaleng.2020.115259>
- Charjouei Moghadam, M., Edalatpour, M., & Solano, J. P. (2017). Numerical study on conjugated laminar mixed convection of alumina/water nanofluid flow, heat transfer, and entropy generation within a tube-on-sheet flat plate solar collector. *Journal of Solar Energy Engineering*, 041011. <https://doi.org/10.1115/1.4036854>
- Choudhary, S., Sachdeva, A., & Kumar, P. (2020). Investigation of the stability of MgO nanofluid and its effect on the thermal performance of flat plate solar collector. *Renewable Energy*, 147, 1801–1814. <https://doi.org/10.1016/j.renene.2019.09.126>
- Dehaj, M. S., & Mohiabadi, M. Z. (2019). Experimental investigation of heat pipe solar collector using MgO nanofluids. *Solar Energy Materials and Solar Cells*, 91–99. <https://doi.org/10.1016/j.solmat.2018.10.025>
- Edalatpour, M., & Solano, J. P. (2017). Thermal-hydraulic characteristics and exergy performance in tube-on-sheet flat plate solar collectors: Effects of nanofluids and mixed convection. *International Journal of Thermal Sciences*, 397–409. <https://doi.org/10.1016/j.ijthermalsci.2017.05.004>
- Ellahi, R., Hassan, M., & Zeeshan, A. (2015). Shape effects of nanosize particles in Cu–H₂O nanofluid on entropy generation. *International Journal of Heat and Mass Transfer*, 81, 449–456. <https://doi.org/10.1016/j.ijheatmasstransfer.2014.10.041>
- Eltaweel, M., Abdel-Rehim, A. A., & Attia, A. A. A. (2021). A comparison between flat-plate and evacuated tube solar collectors in terms of energy and exergy analysis by using nanofluid. *Applied Thermal Engineering*, 186, 116516. <https://doi.org/10.1016/j.applthermaleng.2020.116516>
- Farajzadeh, E., Movahed, S., & Hosseini, R. (2018). Experimental and numerical investigations on the effect of Al₂O₃/TiO₂H₂O nanofluids on thermal efficiency of the flat plate solar collector. *Renewable Energy*, 118, 122–130. <https://doi.org/10.1016/j.renene.2017.10.102>
- Farhana, K., Kadirgama, K., Mohammed, H. A., Ramasamy, D., Samykan, M., & Saidur, R. (2021). Analysis of efficiency enhancement of flat plate solar collector using crystal nanocellulose (CNC) nanofluids. *Sustainable Energy Technologies and Assessments*, 45, 101049. <https://doi.org/10.1016/j.seta.2021.101049>
- Genc, A. M., Ezan, M. A., & Turgut, A. (2018). Thermal performance of a nanofluid-based flat plate solar collector: A transient numerical study. *Applied Thermal Engineering*, 395–407. <https://doi.org/10.1016/j.applthermaleng.2017.10.166>
- Gunjo, D. G., Mahanta, P., & Robi, P. S. (2017). CFD and experimental investigation of flat plate solar water heating system under steady state condition. *Renewable Energy*, 106, 24–36. <https://doi.org/10.1016/j.renene.2016.12.041>
- Gupta, M., Singh, V., Kumar, S., Kumar, S., Dilbaghi, N., & Said, Z. (2018). Up to date review on the synthesis and thermophysical properties of hybrid nanofluids. *Journal of Cleaner Production*, 169–192. <https://doi.org/10.1016/j.jclepro.2018.04.146>
- Hussein, O. A., Habib, K., Muhsan, A. S., Saidur, R., Alawi, O. A., & Ibrahim, T. K. (2020). Thermal performance enhancement of a flat plate solar collector using hybrid nanofluid. *Solar Energy*, 204, 208–222. <https://doi.org/10.1016/j.solener.2020.04.034>
- Khan, A. I., & Valan Arasu, A. (2019). A review of influence of nanoparticle synthesis and geometrical parameters on thermophysical properties and stability of nanofluids. *Thermal Science and Engineering Progress*, 11, 334–364. <https://doi.org/10.1016/j.tsep.2019.04.010>
- Kumar, L. H., Kazi, S. N., Masjuki, H. H., Zubir, M. N. M., Jahan, A., & Bhinitha, C. (2021). Energy, exergy and economic analysis of liquid flat-plate solar collector using green covalent functionalized graphene nanoplatelets. *Applied Thermal Engineering*, 116916.
- Kumar, V., & Sarkar, J. (2019). Numerical and experimental investigations on heat transfer and pressure drop characteristics of Al₂O₃-TiO₂ hybrid nanofluid in minichannel heat sink with different mixture ratio. *Powder Technology*, 345, 717–727. <https://doi.org/10.1016/j.powtec.2019.01.061>
- Kumar, V., & Sarkar, J. (2020a). Experimental hydrothermal behavior of hybrid nanofluid for various particle ratios and comparison with other fluids in minichannel heat sink. *International Communications in Heat and Mass Transfer*, 110, 104397. <https://doi.org/10.1016/j.icheatmasstransfer.2019.104397>
- Kumar, V., & Sarkar, J. (2020b). Particle ratio optimization of Al₂O₃-MWCNT hybrid nanofluid in minichannel heat sink for best hydrothermal performance. *Applied Thermal Engineering*, 165, 114546. <https://doi.org/10.1016/j.applthermaleng.2019.114546>

- Liu, S., Afan, H. A., Aldlemy, M. S., Al-Ansari, N., & Yaseen, Z. M. (2020). Energy analysis using carbon and metallic oxides-based nanomaterials inside a solar collector. *Energy Reports*, 6, 1373–1381. <https://doi.org/10.1016/j.egy.2020.05.015>
- Marulasiddeshi, H. B., Kanti, P. K., Jamei, M., Prakash, S. B., Sridhara, S. N., & Said, Z. (2022). Experimental study on the thermal properties of Al₂O₃-CuO/water hybrid nanofluids: Development of an artificial intelligence model. *International Journal of Energy Research*, 46(15), 21066–21083. <https://doi.org/10.1002/er.8739>
- Minea, A. A. (2017). Challenges in hybrid nanofluids behavior in turbulent flow: Recent research and numerical comparison. *Renewable and Sustainable Energy Reviews*, 71, 426–434. <https://doi.org/10.1016/j.rser.2016.12.072>
- Munyalo, J. M., & Zhang, X. (2018). Particle size effect on thermophysical properties of nanofluid and nanofluid based phase change materials: A review. *Journal of Molecular Liquids*, 265, 77–87. <https://doi.org/10.1016/j.molliq.2018.05.129>
- Okonkwo, E. C., Wole-Osho, I., Kavaz, D., Abid, M., & Al-Ansari, T. (2020). Thermodynamic evaluation and optimization of a flat plate collector operating with alumina and iron mono and hybrid nanofluids. *Sustainable Energy Technologies and Assessments*, 100636. <https://doi.org/10.1016/j.seta.2020.100636>
- Pandey, K. M., & Chaurasiya, R. (2017). A review on analysis and development of solar flat plate collector. *Renewable and Sustainable Energy Reviews*, 641–650. <https://doi.org/10.1016/j.rser.2016.09.078>
- Sahoo, R. R., & Sarkar, J. (2016). Heat transfer performance characteristics of hybrid nanofluids as coolant in louvered fin automotive radiator. *Heat and Mass Transfer*, 53(6), 1923–1931. <https://doi.org/10.1007/s00231-016-1951-x>
- Sarsam, W. S., Kazi, S. N., & Badarudin, A. (2020a). Thermal performance of a flat-plate solar collector using aqueous colloidal dispersions of graphene nanoplatelets with different specific surface areas. *Applied Thermal Engineering*, 115142. <https://doi.org/10.1016/j.applthermaleng.2020.115142>
- Sarsam, W. S., Kazi, S. N., & Badarudin, A. (2020b). Thermal performance of a flat-plate solar collector using aqueous colloidal dispersions of multi-walled carbon nanotubes with different outside diameters. *Experimental Heat Transfer*, 258–281. <https://doi.org/10.1080/08916152.2020.1847215>
- Sheikholeslami, M., Farshad, S. A., Ebrahimpour, Z., & Said, Z. (2021). Recent progress on flat plate solar collectors and photovoltaic systems in the presence of nanofluid: A review. *Journal of Cleaner Production*, 126119. <https://doi.org/10.1016/j.jclepro.2021.126119>
- Singh, S. K., & Sarkar, J. (2018). Energy, exergy and economic assessments of shell and tube condenser using hybrid nanofluid as coolant. *International Communications in Heat and Mass Transfer*, 98, 41–48. <https://doi.org/10.1016/j.icheatmasstransfer.2018.08.005>
- Sint, N. K. C., Choudhury, I. A., Masjuki, H. H., & Aoyama, H. (2017). Theoretical analysis to determine the efficiency of a CuO-water nanofluid based-flat plate solar collector for domestic solar water heating system in Myanmar. *Solar Energy*, 155, 608–619. <https://doi.org/10.1016/j.solener.2017.06.055>
- Sundar, L. S., Ramana, E. V., Said, Z., Punnaiah, V., Mouli, K. V. V. C., & Sousa, A. C. M. (2020). Properties, heat transfer, energy efficiency and environmental emissions analysis of flat plate solar collector using nanodiamond nanofluids. *Diamond and Related Materials*, 110, 108115. <https://doi.org/10.1016/j.diamond.2020.108115>
- Tao, H., Alawi, O. A., Hussein, O. A., Ahmed, W., Abdelrazek, A. H., Homod, R. Z., Eltaweel, M., Falah, M. W., Al-Ansari, N., & Yaseen, Z. M. (2022). Thermohydraulic analysis of covalent and noncovalent functionalized graphene nanoplatelets in circular tube fitted with turbulators. *Scientific Reports*, 12(1), 17710. <https://doi.org/10.1038/s41598-022-22315-9>
- Timofeeva, E. V., Routbort, J. L., & Singh, D. (2009). Particle shape effects on thermophysical properties of alumina nanofluids. *Journal of Applied Physics*, 106(1), 014304. <https://doi.org/10.1063/1.3155999>
- Tong, Y., Chi, X., Kang, W., & Cho, H. (2020). Comparative investigation of efficiency sensitivity in a flat plate solar collector according to nanofluids. *Applied Thermal Engineering*, 115346. <https://doi.org/10.1016/j.applthermaleng.2020.115346>
- Verma, S. K., Tiwari, A. K., & Chauhan, D. S. (2017). Experimental evaluation of flat plate solar collector using nanofluids. *Energy Conversion and Management*, 134, 103–115. <https://doi.org/10.1016/j.enconman.2016.12.037>
- Verma, S. K., Tiwari, A. K., Tiwari, S., & Chauhan, D. S. (2018). Performance analysis of hybrid nanofluids in flat plate solar collector as an advanced working fluid. *Solar Energy*, 167, 231–241. <https://doi.org/10.1016/j.solener.2018.04.017>
- Xiong, Q., Altnji, S., Tayebi, T., Izadi, M., Hajjar, A., Sundén, B., & Li, L. K. B. (2021). A comprehensive review on the application of hybrid nanofluids in solar energy collectors. *Sustainable Energy Technologies and Assessments*, 47, 101341. <https://doi.org/10.1016/j.seta.2021.101341>
- Yang, L., Ji, W., Mao, M., & Huang, J. (2020). An updated review on the properties, fabrication and application of hybrid-nanofluids along with their environmental effects. *Journal of Cleaner Production*, 257, 120408. <https://doi.org/10.1016/j.jclepro.2020.120408>
- Zayed, M. E., Zhao, J., Du, Y., Kabeel, A. E., & Shalaby, S. M. (2019). Factors affecting the thermal performance of the flat plate solar collector using nanofluids: A review. *Solar Energy*, 182, 382–396. <https://doi.org/10.1016/j.solener.2019.02.054>
- Ziyadanogullari, N. B., Yucel, H. L., & Yildiz, C. (2018). Thermal performance enhancement of flat-plate solar collectors by means of three different nanofluids. *Thermal Science and Engineering Progress*, 8, 55–65. <https://doi.org/10.1016/j.tsep.2018.07.005>